Proceedings of the ASME Fluids Engineering Summer Meeting
FEDSM2013
July 7-11, 2013, Incline Village, Nevada, USA

FEDSM2013-16116

EFFECT OF AMPLITUDE ON MASS TRANSPORT, VOID FRACTION AND BUBBLE SIZE IN A VERTICALLY VIBRATING LIQUID-GAS BUBBLE COLUMN REACTOR

A.L. Still and A.J. Ghajar*
School of Mechanical and Aerospace Engineering
Oklahoma State University
Stillwater, Oklahoma, USA

T.J. O'Hern
Engineering Sciences Center
Sandia National Laboratories
Albuquerque, New Mexico, USA

ABSTRACT

Two-phase and three-phase Bubble Column Reactors are used in many chemical, petroleum, and bio-systems processing applications such as the hydrogenation of coal slurry to produce synthetic fuels during the Fischer-Tropsch process. Vertical vibration of a Bubble Column Reactor has previously been shown to increase mass transfer, increase void fraction, decrease bubble size and establish interesting flow phenomena through kinetic buoyancy or "Bjerknes force". However, the effect of kinetic buoyancy on the flow field, mass transfer, and flow properties such as void fraction is not fully understood. While previous research has focused on the effect of vibration frequency ($10 < f < 120$ Hz) at low amplitudes, ($A < 2.5$ mm) very little attention has been given to the effect of larger amplitudes. Therefore, a new experimental set up was designed, built, verified by comparison to previous research, and used to collect mass transfer, void fraction, and bubble size data at high amplitude ($2.5 \text{ mm} < A < 9.5 \text{ mm}$) over a frequency range of 7.5-22.5 Hz. Comparison of the results with previous research shows similar local maxima occurring for void fraction and mass transfer, but that an optimum amplitude may exist for mass transfer which is independent of frequency. Statistical analysis and comparison of the results with data from the literature suggests a stronger relationship may exist between kinetic buoyancy and mass transfer than previously theorized.

INTRODUCTION

There are many applications for Bubble Column Reactors (BCRs) including aeration of organic organisms in bio-reactors, hydrogenation of coal-slurries to produce synthetic fuels used in the Fischer-Tropsch process, and gasification of solvent for chemical reactions.

It was discovered in the early 1960's that vibration could help improve efficiency in BCR processes by increasing the mass transfer rate [1-4]. Some additional research expanded the theory [5-7], but it was not until the early 2000's that the science was reinvigorated [8-16]. Recent research has gone so far as to develop theoretical, physics based models to try and predict mass transfer and void fraction in BCR systems undergoing vibration [14-15]. These models were tested in a limited manner, but have yet to be fully understood or validated against a large body of experimental data.

Therefore, a fundamental understanding of the multiphase flow properties such as void fraction and bubble size distribution as well as the related mass transfer properties are crucial to understanding and thereby improving the operation of BCRs. It is with this concept in mind that the current research is carried out.

A common method to measure the volumetric mass transfer coefficient, $k_L a$, in a BCR is to solve the transient mass balance for the whole column (batch) leading to Eq. (1) [7-16],

$$\frac{dC}{dt} = k_L a\left(C^* - C\right) \tag{1}$$

where C is the instantaneous concentration of dissolved gas in the liquid, C^* is the saturation concentration and t represents time. Provided the BCR is assumed to be well-mixed (i.e. concentration is uniform throughout the batch), measurement of the instantaneous oxygen concentration of the liquid at any point in the column is representative of the batch. BCRs are generally assumed to be well-mixed due to the level of turbulence within the liquid column.

The void fraction is defined as the ratio of volume occupied by the gas phase to the total volume in a multiphase system. The BCR is considered a batch system and as such the void fraction can be measured by,

* Corresponding author; afshin.ghajar@okstate.edu

$$\varepsilon = 1 - \frac{H_0}{H} \tag{2}$$

where H_0 is the stagnant liquid column height and H is the dynamic air-liquid interface height [7-11].

There have been various attempts to classify the size of the bubbles by a characteristic length. A few researchers have measured bubble chord length, and they presented the bubble size as a probability distribution with a representative mean diameter [17-19]. The advantage of this method is that it does not have to rely on the assumption of a spherical bubble. Many researchers, however, prefer to use a mean bubble diameter based upon the Sauter mean diameter (d_{32}) calculated as the ratio of the representative bubble volume to the bubble area Eq. (4) [5, 14-16, 20]. For instance the Sauter mean diameter is usually preferred when photographic methods are used. In order to do so, however, an equivalent diameter must be derived from a 2D bubble area measurement [18] following Eq. (3).

$$d_{eq} = \sqrt{\frac{4}{\pi} A_{proj}} \tag{3}$$

$$d_{32} = \frac{\sum_{i=1}^{n} n_i d_{b,i}^3}{\sum_{i=1}^{n} n_i d_{b,i}^2} \tag{4}$$

The oscillating pressure field in the fluid at a particular column height can be defined by [5, 14-15],

$$p_T = p_e + \rho_L g h - \rho_L h \omega^2 A \sin \omega t \tag{5}$$

where, p_T is the total pressure, p_e is the external pressure, ρ_L is the liquid density, h is the liquid height above the bubble, A is the oscillation amplitude, ω is the angular frequency, g is gravitational acceleration, and t is time. It is easily seen that the combined terms in Eq. (5) are the hydrostatic and vibrational pressures respectively. Assuming isothermal expansion and contraction and ignoring surface tension effects for small bubbles the bubble volume can be defined by [15],

$$V = V_0 + \Delta V_{\max} \sin \omega t \tag{6}$$

where V_0 is the mean bubble volume and $\Delta V_{\max}$ is the maximum change in bubble volume. Using Boyle's Law and assuming: 1) bubble resonant frequency is much greater than the column oscillation frequency and 2) bubble volume oscillation is in phase with fluid pressure (column vibration frequency) the critical frequency is related to the dynamic volume of the bubble, fluid properties, and the motion of the fluid as follows,

$$\frac{\Delta V_{\max} \sin(\omega t)}{V_0} = \frac{\rho_L h \omega^2 A \sin(\omega t)}{p_e + \rho_L h g - \rho_L h \omega^2 A \sin(\omega t)} \tag{7}$$

A maximum volume can be considered when fluid pressure is minimum at which point the *sin* terms are unity. Thus, Waghmare et al. [14-15] use Eq. (7) to derive Eq. (8) by assuming that external pressure must be much larger than the difference between the hydrostatic and dynamic pressure.

$$\frac{\Delta V_{\max}}{V_0} = \frac{\rho_L h \omega^2 A}{p_e} \tag{8}$$

It should be noted at this point that this assumption is not entirely accurate, but makes the derivation of Bjerknes number, *Bj*, cleaner. Note that for a typical test point at H_L = 78 cm, p_0 = 1 atm, f = 27 Hz and A = 2.5 mm, the ratio becomes,

$$\frac{p_e}{\left|\rho_L g h - \rho_L h \omega^2 A\right|} \approx 2 \tag{9}$$

However, this assumption breaks down as frequency approaches 40 Hz and Eq. (9) goes to 1. The body of this work and that of Waghmare et. al. [14-15] stays below f = 25 Hz so the assumption is valid. An instantaneous force balance on the sinusoidally oscillating bubble in a sinusoidally oscillating pressure field (neglecting drag) is given by [5, 14-15, 21],

$$F(t) = \rho_L (V_0 + \Delta V_{\max} \sin \omega t) g - \rho_L (V_0 + \Delta V_{\max} \sin \omega t) \omega^2 A \sin \omega t \tag{10}$$

Integration of Eq. (10) over a complete cycle (period) results in a time averaged force balance in which Eq. (8) can be substituted to derive,

$$F = \rho_L V_0 g \left[1 - Bj(h)\right] \tag{11}$$

where Bjerknes number, *Bj(h)*, is defined as,

$$Bj(h) = \frac{1}{2} \frac{\rho_L h \omega^4 A^2}{g p_e} \tag{12}$$

Bj is dimensionless, and provides a unique parameter in which a theoretical bubble's velocity goes to zero and can be considered stabilized at a specific column height when *Bj* = 1 [5, 14-15, 22]. *Bj* has also been attributed as a parameter influencing mass transfer and void fraction [10-16]. For a more thorough review of the derivation see [5, 14-16].

Waghmare et al. [14-15] extends the use of *Bj* by adding a drag term and building from Eq. (11) to form a column average void fraction model given by,

$$\varepsilon = 2.25\left[\frac{U_{SG}(P_m)^{2/5}}{\left(\frac{\sigma}{\rho_L}\right)^{3/5}\left(\frac{g}{\sqrt{\nu}}\right)^{2/3}}\right]E(Bj) \qquad (13)$$

$$E(Bj) = \frac{3}{Bj}\left[1-(1-Bj)^{1/3}\right]$$

The model assumes: 1) volumetric interfacial area is a function of void fraction, 2) rise velocity is a function of superficial gas velocity, and 3) viscous drag coefficient based upon a fluidized bed.

A column average volumetric mass transfer coefficient equation can be derived based on Eq. (13) and a penetration theory of diffusion given by [14-16, 23],

$$k_L a = 4.58\left[\frac{U_{SG}\sqrt{\mathcal{D}}P_m^{\,4/5}}{\left(\frac{\sigma}{\rho_L}\right)^{6/5}\left(\frac{g}{\sqrt{\nu}}\right)^{1/3}}\right]G(Bj) \qquad (14)$$

$$G(Bj) = \frac{3}{2}\left[\frac{1-(1-Bj)^{2/3}}{Bj}\right]$$

where Bj in both Eq. (13) and Eq. (14) is given by Eq. (12) with h = the total column liquid height, H, and P_m in Eq. (14) is the specific power input (W/kg) defined by,

$$P_m = gU_{SG} + \frac{1}{2}A^2\omega^3 \qquad (15)$$

Eqs. (13-14) were tested using mass transfer and void fraction data from a piston pulsed BCR at amplitudes of 1.66 and 2.46 mm [14-16]. In addition, previous research has primarily focused on mass transfer, void fraction and bubble size for small amplitudes (A < 2.5 mm) and at high frequencies (f > 20 Hz) [7-15]. While previous research has primarily been concerned with frequency effects, some results have indicated increasing amplitude may account for greater improvements at lower power requirements [10, 13]. Therefore, it is the intent of this research to investigate the effect increasing amplitude has on mass transport as perceived through the volumetric mass transfer coefficient k_La, void fraction ε, and bubble size d_{32}.

EXPERIMENTAL

Equipment

The experimental setup is comprised of two components, namely the shaker and an instrumented BCR. The shaker design is similar to that used by Buchanan et al. [5] because of similar experimental ranges. The shaker imparts the necessary vibration to the BCR and consists of a platform to which the entire bubble column is mounted and an adjustable eccentric drive mechanism and linkage. The amplitude of the shaker platform is provided by an adjustable eccentric mechanism and provides amplitudes of 0.1-10 mm. The shaker is powered by a 3 phase, 3 hp, 208-239 volts alternating current, WEG motor and the vibration frequency imparted to the BCR is controlled by a Schneider Electric variable frequency drive which controls the speed of the motor. The shaker was designed for a frequency range of 7.5-50 Hz. An accelerometer was mounted to the shaker platform to periodically confirm both the vertical vibration input and any out of axis vibration to the BCR from the shaker.

The BCR was made from a 48 inch long, clear cast acrylic tube with a 4 inch internal diameter. The tube was mounted vertically on the platform and sealed at both ends. A removable seal at the top allowed the tube to be filled with distilled water. Two pressure taps were installed in the tube at the 79 and 1019 mm fluid column heights and connected to a Validyne differential pressure transducer to measure the oscillating fluid pressure during vibration. The pressure inside the column was controlled by a pressure manifold and relief valve and supplied by compressed air or vacuum pump as needed. The complete experimental set up is shown in Fig. 1.

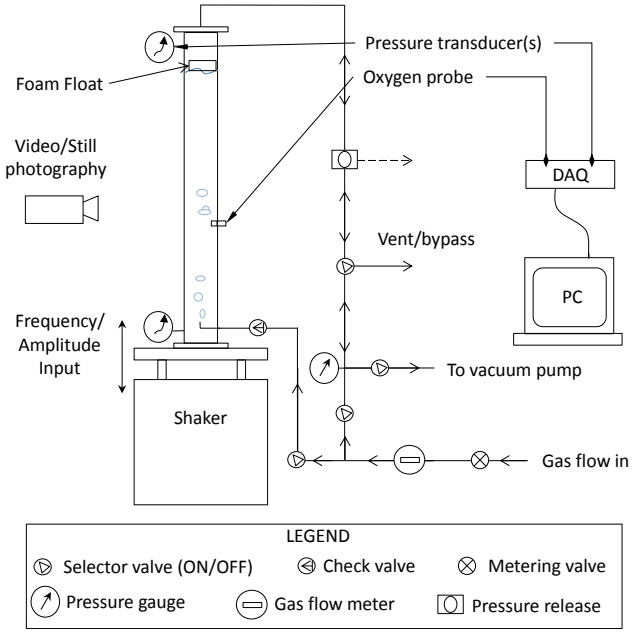

FIGURE 1. Experimental set up

A 15 gauge, 316 stainless steel, hypodermic round tube with a nominal 0.0625 inch (1.53 mm) inner diameter was used to inject filtered, compressed air into the fluid. The single point injector height was 58.5 mm from the insertion point on the column, but all column fluid height measurements were taken relative to the injector tip (H_L = 0 cm). Gas flow rate to the

injector was measured using a Micro Motion Elite Coriolis mass flow meter with a range of 0.0002-0.0062 ± 0.20% kg/min. The flow rate was controlled using a coarse metering valve in series with a Parker Vernier type needle valve for fine adjustments. The Coriolis mass flow meter was also used to measure the gas temperature. A Vernier dissolved oxygen (DO) probe with a resolution of 0.007 mg/L and uncertainty of ± 0.2 mg/L was used to measure the dissolved oxygen concentration for mass transfer measurements. The DO probe was installed 3 column diameters above the injector tip and 0.1 diameters from the column wall to account for mixing length and wall effects [24, 25].

Instrument measurements were collected by a 13 bit Vernier SensorDAQ digital to analog converter connected to a PC. A Nikon D3100 digital camera and a telescoping tripod were used to capture 9.8 MB monochrome still images of the bubbles. A Casio Exilim EX-F1 was used to capture video at a rate of 300 frames per second, and a Sony DCR-VX2000 video camera was used to capture traditional video at 30 frames per second.

Methodology

Mass transfer coefficient, void fraction and bubble size measurements were taken for a liquid column height, H_L = 85 cm using distilled water. Air was injected into the column at superficial gas velocities of 1.0, 2.5, 5.0, 7.5, and 10.0 mm/s. Two experiment sets were performed at these gas flow rates. The first set was conducted to validate the experimental set up against published research data, and the second to investigate the effects of large amplitude vibration. For the first set, vibration frequencies of 0, 10, 12.5, 15, 17.5, 20 and 22.5 Hz and amplitudes of 1.5 and 2.5 mm were tested, which closely follow the conditions of Waghmare [14-16]. The second set consisted of testing at amplitudes of 4.5, 6.5, and 9.5 mm over a frequency range of 7.5-17.5 Hz, which had not been investigated in the literature.

The mass transfer coefficient k_La was determined by the "unsteady state" method used in [7-15]. The oxygen concentration was measured over time and an exponential regression of the data was performed to derive k_La using the following equations:

$$-\ln(C') = k_L a t \tag{16}$$

where C' is a dimensionless, instantaneous concentration $C(t)$ defined by,

$$C' = \frac{C^* - C(t)}{C^* - C_0} \tag{17}$$

The gas mass flow rate was set to meet the desired superficial gas velocity U_{SG}, and allowed to reach a steady state prior to application by bypassing the injector. Data acquisition was started first in order to establish an initial concentration C_0. The shaker was then started and allowed to reach a steady speed. Gas flow was then directed to the injector. U_{SG} was determined by taking the column average density of the gas bubbles by,

$$\langle \rho_G \rangle = \frac{\langle p_G \rangle}{\langle T_G \rangle R_{air}} \tag{18}$$

$$\langle U_{SG} \rangle = \frac{\dot{m}_G}{\langle \rho_G \rangle A_{CS}} \tag{19}$$

where $\langle p_G \rangle$ is taken as the total pressure at mid-column (H_L = 42.5 cm), and R_{air} = 287 J/kg-K.

Oxygen concentration was then recorded until the fluid saturation was approximately 95% complete which corresponds to a time equivalent of 3τ where,

$$\tau = \frac{1}{k_L a} \tag{20}$$

Column average void fraction ε was calculated by a volumetric method using the liquid-air interface height (H) described by Eq. (2). Still images and a foam float were used to assist in the determination of H [13]. The foam float was measured before and after testing with no significant change in mass and weighed only 7 grams. Therefore, it was assumed the float did not adversely affect the dynamics of the system. Multiple photographs were taken of the column head and the distance from the known stagnant liquid height (H_0) to the float (H) was measured with ImageJ software. The pixel scale was determined for each image separately using a known distance reference on the column. Hence, each image used was individually calibrated to reduce focal length error. An average H was determined from the processed image data.

Bubble size (d_{32}) was measured by still images using similar techniques found in the literature [14, 20]. A series of pictures (10+) were taken at each column height, H_L = 30, 45 and 60 cm, to determine any height dependencies that may exist. Monochrome pictures were taken of bubbles at a shutter speed of 1/4000 seconds. In order to reduce optical distortion from the column wall, images were taken from a mid-column cross section. Each of the three image sets was taken during a single run. ImageJ software was used to produce a 2D area measurement for each significant bubble per image in the image set. Each image set was calibrated with a pixel scale by measurement of a known reference distance on the column. The 2D area measurements were then converted to an equivalent spherical diameter in order to calculate d_{32}. The flow visualization set up used to produce both air-water interface and bubble images is shown in Fig. 2.

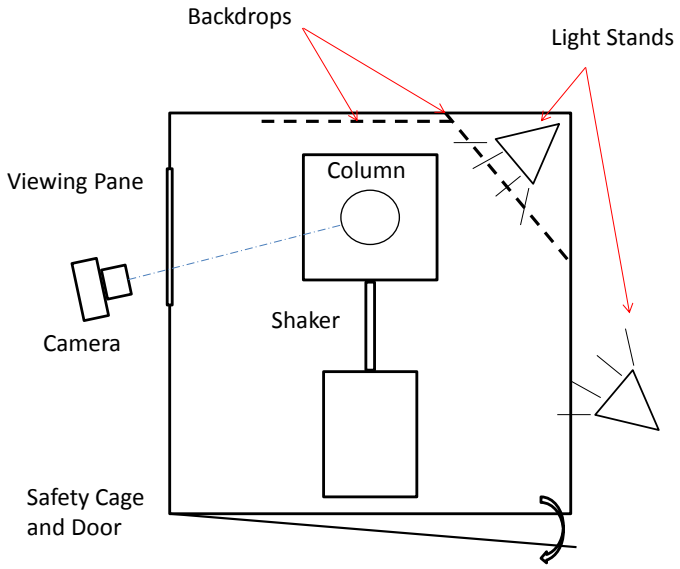

FIGURE 2. Flow visualization schematic

RESULTS AND DISCUSSION

Mass transfer coefficient

The appearance of significant mass transfer and void fraction improvement at particular frequencies, excitation modes, has been identified previously [11-15]. Mass transfer coefficients for dynamic conditions were found to agree with those of Waghmare [16] (Fig. 3), especially in trends and location of excitation modes (f = 17.5 Hz) for similar conditions (A = 2.5 mm, U_{SG} = 2.5 mm/s) (Fig. 3). The magnitudes of k_La are comparable for U_{SG} = 2.5 mm/s with worst case 35% difference at f = 20 Hz (Fig. 3). It is important to note that f = 20 Hz, A = 2.5 mm was a significantly difficult point to collect due to a repeatable, uncharacterized response of the set up at that frequency. Additional points were taken at f = 19 Hz and f = 21 Hz (U_{SG} = 5.0 mm/s) to examine the variation around this critical frequency, and both k_La values were found to be within 2% of each other. However, both k_La values at f = 19 Hz and f = 20 Hz were at least 8% larger than k_La at f = 20 Hz. The reason for the dip in k_La at f = 20 Hz was not investigated, but the same phenomena occurs in Waghmare [16] at the same frequency. The magnitude of k_La was also comparable at U_{SG} = 5.0 mm/s for f < 17.5 Hz, but began to separate at higher frequencies. The similarity between the results of this research and Waghmare [16] (Fig. 3) also suggests that piston pulsing and whole column shaking produce similar k_La results, especially at lower frequencies (f < 17.5 Hz). This latter conclusion has larger implications toward full-scale vibrating reactor design and implementation. Piston pulsing usually implies smaller shaker component (linkages, bearings, etc.) loads and stress due to decreased oscillating mass, especially when compared to whole column shaking where platform, cylinder, and accessory mass must be carried by the shaker. However, more comprehensive data would be needed for both piston pulsing and whole column shaking set ups to fully understand the difference and the impact the two vibration methods have on k_La and void fraction results.

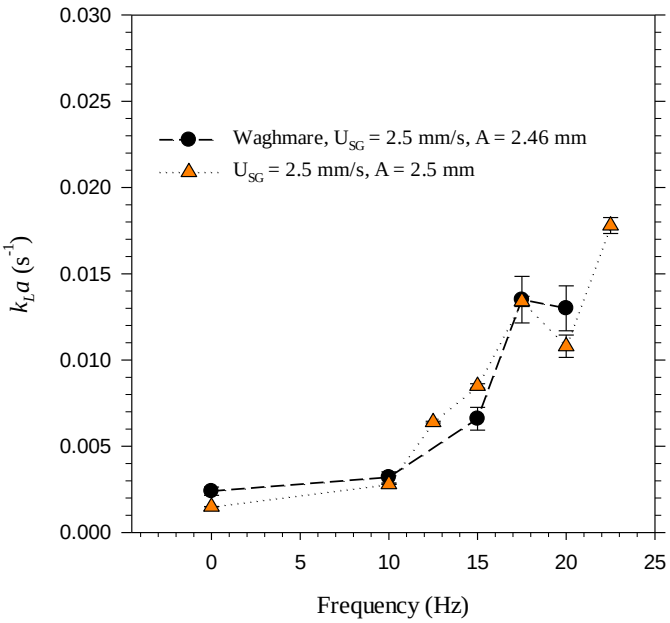

FIGURE 3. Comparison of k_La vs. f with Waghmare [16] for similar vibration conditions at U_{SG} = 2.5 mm/s

The results of the mass transfer experiments carried out for vibration amplitude, A = 4.5–9.5 mm show the same modal similarities as observed at lower amplitudes in that certain frequency-amplitude combinations produce local maxima. The values reached for k_La at high amplitude were also generally higher than those for lower amplitudes at the same frequencies (Table 1).

TABLE 1. Mass transfer improvement ratio k_La/k_La_0 for U_{SG} = 5.0 mm/s

f (Hz)	Amplitude (mm)				
	1.5	2.5	4.5	6.5	9.5
7.5	-	-	-	2.7	4.0
10.0	1.5	2.0	2.6	2.9	2.3
12.5	2.1	2.7	6.6	6.8	6.9
15.0	2.5	5.5	5.8	10.2	6.0
17.5	2.9	7.6	8.3	-	-
20.0	4.4	6.2	-	-	-
22.5	-	7.0	-	-	-

However, the improvement ratio, k_La/k_La_0 appears to stall when the non-dimensional amplitude A/d_i > 4 (where d_i is the gas injector internal diameter), as seen in Fig. 4. While the general trend of all the curves in Fig. 4 denote a global maximum, there are local maxima that occur, such as at f = 15

Hz and $A/d_i \approx 1.5$. These local maxima may be caused by the measurement error, but it is more likely that the local maxima are actually caused by the unique frequency/amplitude combination in which the column is "tuned" to an excitation mode as mentioned previously. The presence of a global maximum, however, suggests that an optimum amplitude exists, independent of frequency, within the frequency range tested. Even with the suggestion of an optimum amplitude, nearly equivalent mass transfer coefficients can be found at other frequency/amplitude combinations. An example is presented to illustrate the necessity to optimize the frequency/amplitude combination for k_La. Both f = 12.5 Hz, A = 4.5 mm and f = 22.5 Hz, A = 2.5 mm produce nearly equivalent k_La, which represents an 80% increase in amplitude traded for a 44% reduction in frequency. This trade gives a 44% reduction of vibration power P_v, where P_v is the input vibration power taken as the mass specific integral of force times the velocity over a quarter period or,

$$P_v = \frac{A^2\omega^3}{2} \tag{21}$$

Ultimately, this example serves to emphasize the need for a model that includes unifying parameters composed of frequency/amplitude combinations that can predict and optimize mass transfer in a vibrating BCR system.

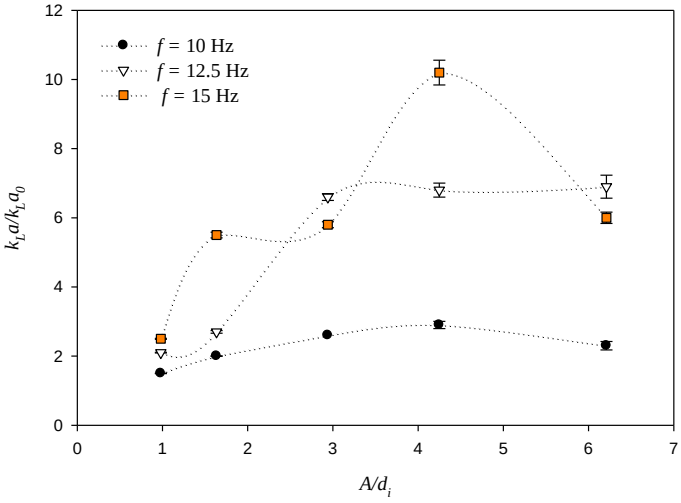

FIGURE 4. Mass transfer improvement with increasing non-dimensional amplitude for f = 10, 12.5, and 15 Hz and U_{SG} = 5.0 mm/s

The work of Waghmare et al. [14-15] have contributed a physics based model that has been supported in part by limited experimental evidence. The model appears at first glance to be appropriate and would support the theory that specific power P_m and superficial gas velocity U_{SG} are the primary factors in mass transfer [7, 13-15] as given by the expression:

$$k_La \propto P_m^{0.8} U_{SG} \tag{22}$$

However, regression of the data from the present research shows that Bj is a stronger factor than P_m. Upon further investigation, Waghmare's data also shows the same result. A simple hypothesis test (t-test) on the exponents of the P_m terms compared to the theoretical exponential value of 0.8 found in Eq. (22) indicates that none of the regression results using Waghmare's data are statistically equal to the exponent (Fig. 5). Taken together with the U_{SG} data, as in Eq. (22), regression of the data gives,

$$k_La \propto P_m^{0.56} U_{SG}^{0.87} \tag{23}$$

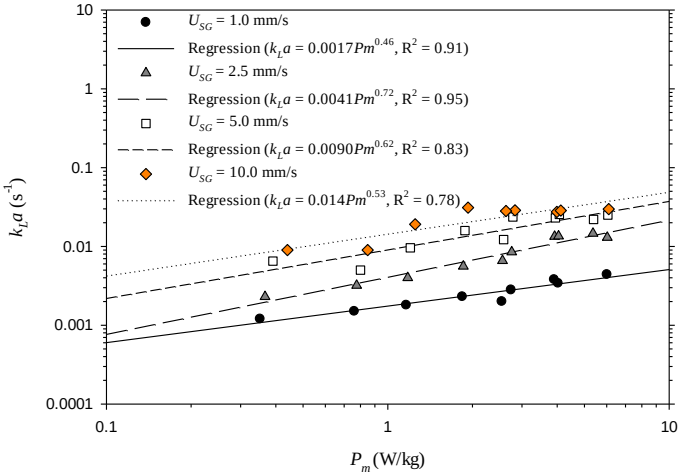

FIGURE 5. Regression results of Waghmare [16] for U_{SG} = 1.0-10.0 mm/s

Using Minitab, linear regressions and ANOVA analyses were performed on both data from Waghmare [16] and the present research. There are three terms in Eq. (14) which can be analyzed separately for independent influences on mass transfer coefficient, namely U_{SG}, P_m, and Bj. The effect of U_{SG} can be neglected by assuming it has a linear contribution to the overall result allowing P_m and Bj to be analyzed independently. Surprisingly, analyses show that Bj is a more appropriate factor to predict k_La over P_m for both data sets (Fig. 6). Independent, linear regression of both data sets as a function of Bj gives exponential values that are statistically equivalent. Therefore, P_m may not be as significant a factor as initially proposed.

A linear ANOVA was performed on Waghmare's data [16] and included all factors and combinations of U_{SG}, P_m, and Bj. The results of the ANOVA provide a correlation (Eq. 24) which deviates from the model proposed (Eq. 14). Correlation of Waghmare's data shows Bj to be the most significant term, and

inverts the relationship of P_m. Additionally, the results of the present research agree well with the correlation of Eq. (24) as shown in Fig. 7.

$$k_L a = K U_{SG}^{0.91} Bj^{0.74} P_m^{-0.46} \quad (24)$$

where K is a constant term related to the experimental conditions and fluid properties, here $K = 0.015$.

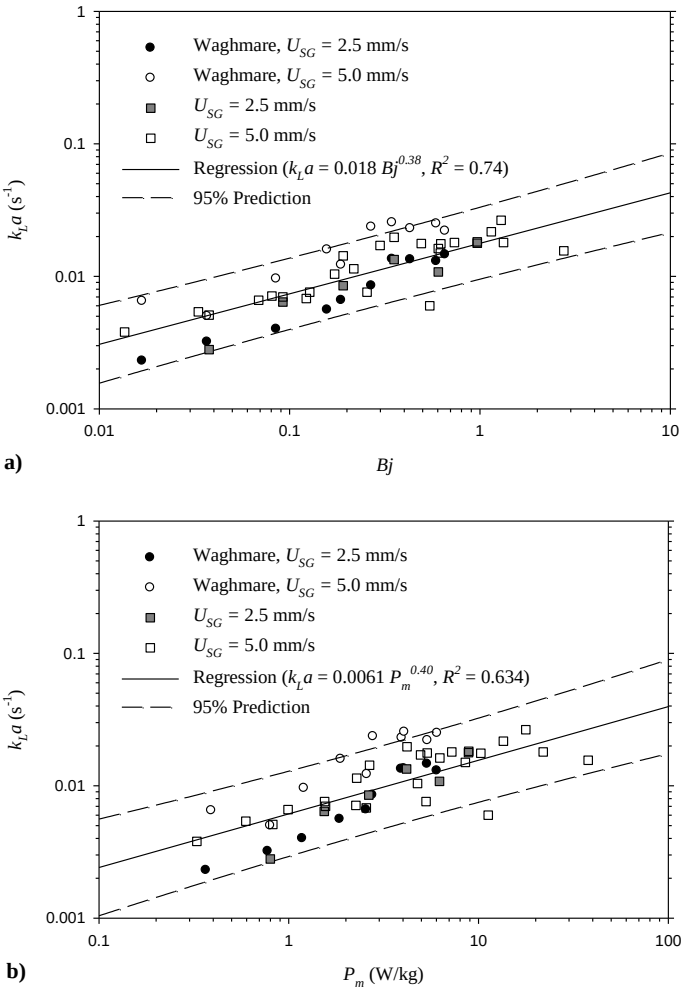

FIGURE 6. Comparative effect of a) Bj and b) P_m on $k_L a$ for the present research and Waghmare [16]

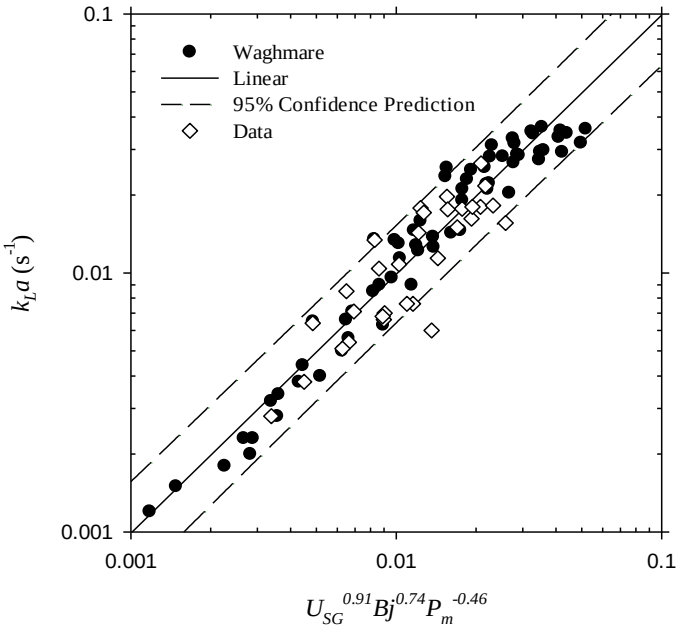

FIGURE 7. Regression correlation of Waghmare [16] data and results of the present research

Void fraction

Void fraction measurements were taken for frequencies of 0-22.5 Hz, amplitudes of 1.5 and 2.5 mm and superficial gas velocities of 1.0–10.0 mm/s. The results are similar to those found for mass transfer, namely that the trends and the magnitudes were similar to Waghmare [16] (Fig. 8).

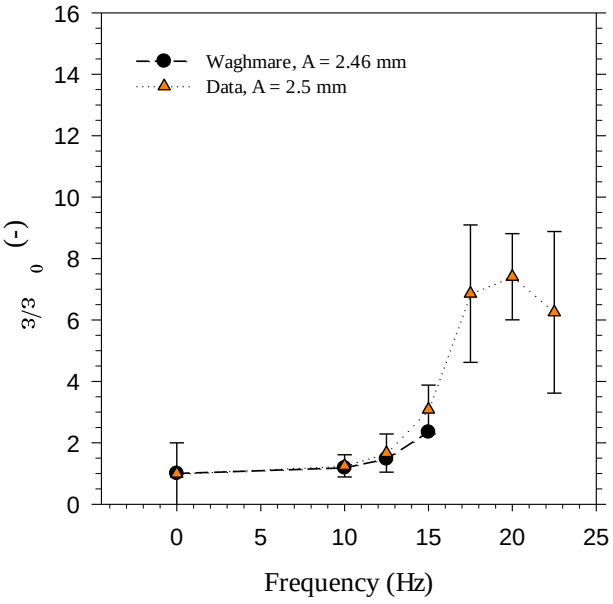

FIGURE 8. Comparison of void fraction improvement ($\varepsilon/\varepsilon_0$) vs. frequency with Waghmare [16] for U_{SG} = 5.0 mm/s

At large amplitudes, A = 2.5-9.5 mm, the presence of maxima occur in the void fraction data similar to k_La, although void fraction increase, $\varepsilon/\varepsilon_0$, with increasing amplitude and frequency are greater than those of mass transfer and do not show a reduction after $A/d_i > 4.25$. The results also show that for the range of frequency tested only one optimum amplitude exists at f = 20 Hz. However, there was larger error at higher frequency/amplitude combinations due to the turbulence at the air-water interface and it is uncertain whether the optimum frequency was at f = 20 Hz. The steady rise in void fraction with non-dimensional amplitude is more clearly seen in Fig. 9. This steady rise of void fraction agrees with a steady reduction in bubble size. However, the presence of a diminishing k_La/k_La_0 values for $A/d_i > 4.25$ (Fig. 4) indicates that improving k_La is not simply increasing the specific interfacial area, a but rather an improvement in k_L dependent upon the frequency/amplitude combinations leading to a tuned column. This independent effect of frequency on k_L has been reported in previous work [2].

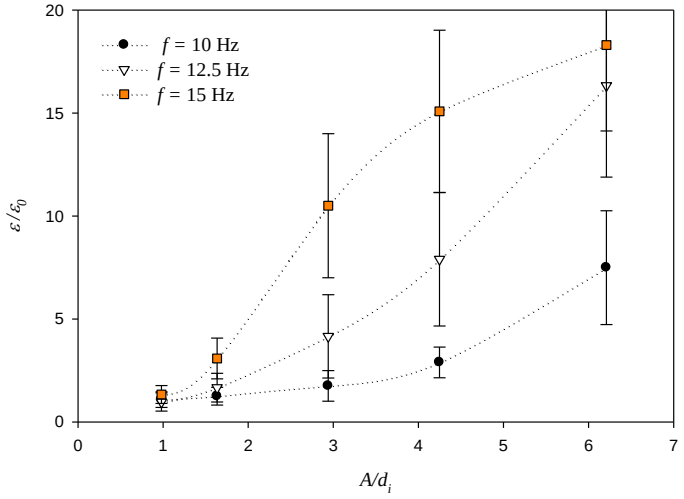

FIGURE 9. Effect of increasing non-dimensional amplitude on void fraction

Minitab was used again to perform linear regressions and ANOVA analyses on both void fraction data from Waghmare [16] and the present research. Unlike results for mass transfer, Waghmare et al. [14-15] void fraction results agree fairly well with theory as given by Eq.'s (13) and (25):

$$\varepsilon \propto P_m^{0.4} U_{SG} \tag{25}$$

However, regression of the data from the present research shows a marked difference from Waghmare and Eq. (25) as given in Eq. (26) (correlation coefficient, R^2 = 0.89):

$$\varepsilon = KBj^{0.97} U_{SG}^{0.16} P_m^{-0.33} \tag{26}$$

where K is a constant term related to the experimental conditions and fluid properties, here K = 0.23.

The difference in void fraction results are likely attributable to the error involved in the measurement of void fraction data. BCR vibration at higher amplitudes often resulted in increased instability and turbulence at the air-water interface (Fig. 11). The increased turbulence affected the stability of the float marker which may have led to exaggerated void fraction measurements.

Bubble Size

Bubble size results show that the Sauter mean diameter, d_{32} decreases with increasing vibration amplitude as seen in Fig. 12. The average measured bubble size with increasing amplitude did not indicate any optimum amplitude as obvious as k_La results (Fig. 10). However, d_{32} at f = 15 Hz, $A/d_i \approx 3$ certainly indicates a larger size reduction than the other frequencies, but occurs at lower amplitude than seen for k_La in Fig. 4. Mass transfer improves as the average bubble size decreases, but certainly increasing surface area due to decreasing bubble size is not the only factor contributing to k_La improvement as indicated by the mismatch of smallest bubble size at $A/d_i \approx 3$ and peak k_La/k_La_0 at $A/d_i \approx 4.25$ and the contrary indication that d_{32} continues to decrease in Fig. 10 while k_La/k_La_0 is seen to decrease for $A/d_i > 4.25$ (Fig. 4).

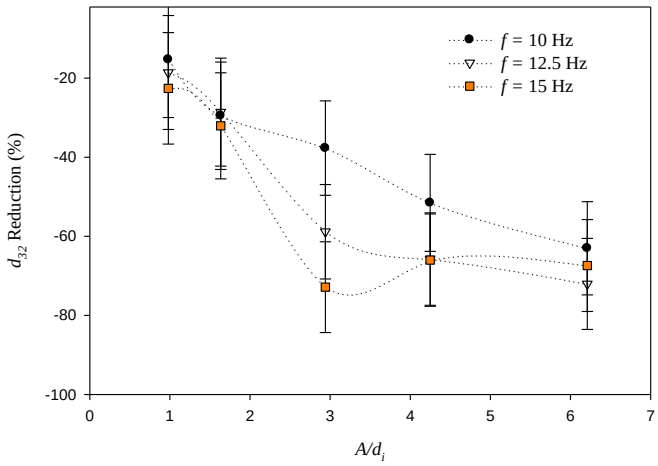

FIGURE 10. Sauter mean diameter reduction vs. non-dimensional amplitude for f = 10, 12.5, 15 Hz

The bubble size distributions also provide an interesting result. In previous research the bubble distributions taken from photographs were reported to take on a normal distribution [15]. However, in this research, the majority of the bubble size distributions were representative of log-normal rather than Gaussian distributions (Fig. 13) as confirmed by the strong linearity indicated on a log-normal probability plot (Fig. 14). These results are similar to the size distribution of samples taken with direct measurement techniques such as the 4 point optical probe for static BCRs [17-19].

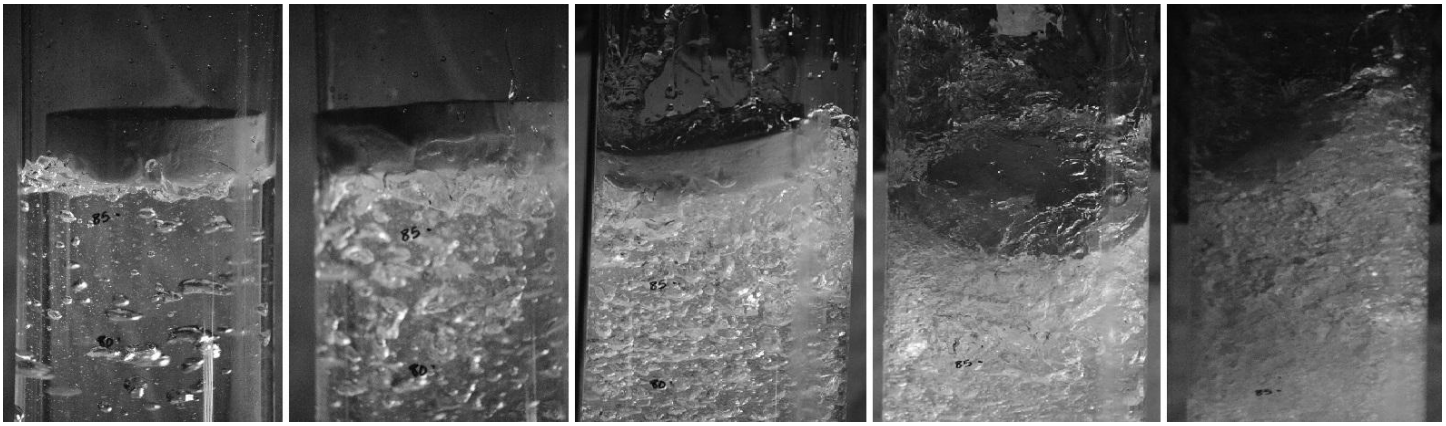

Figure 11: Air-Water interface at f = 12.5 Hz and (from left to right) A = 1.5 mm, 2.5 mm, 4.5 mm, 6.5 mm, 9.5 mm (H_0 = 85 cm)

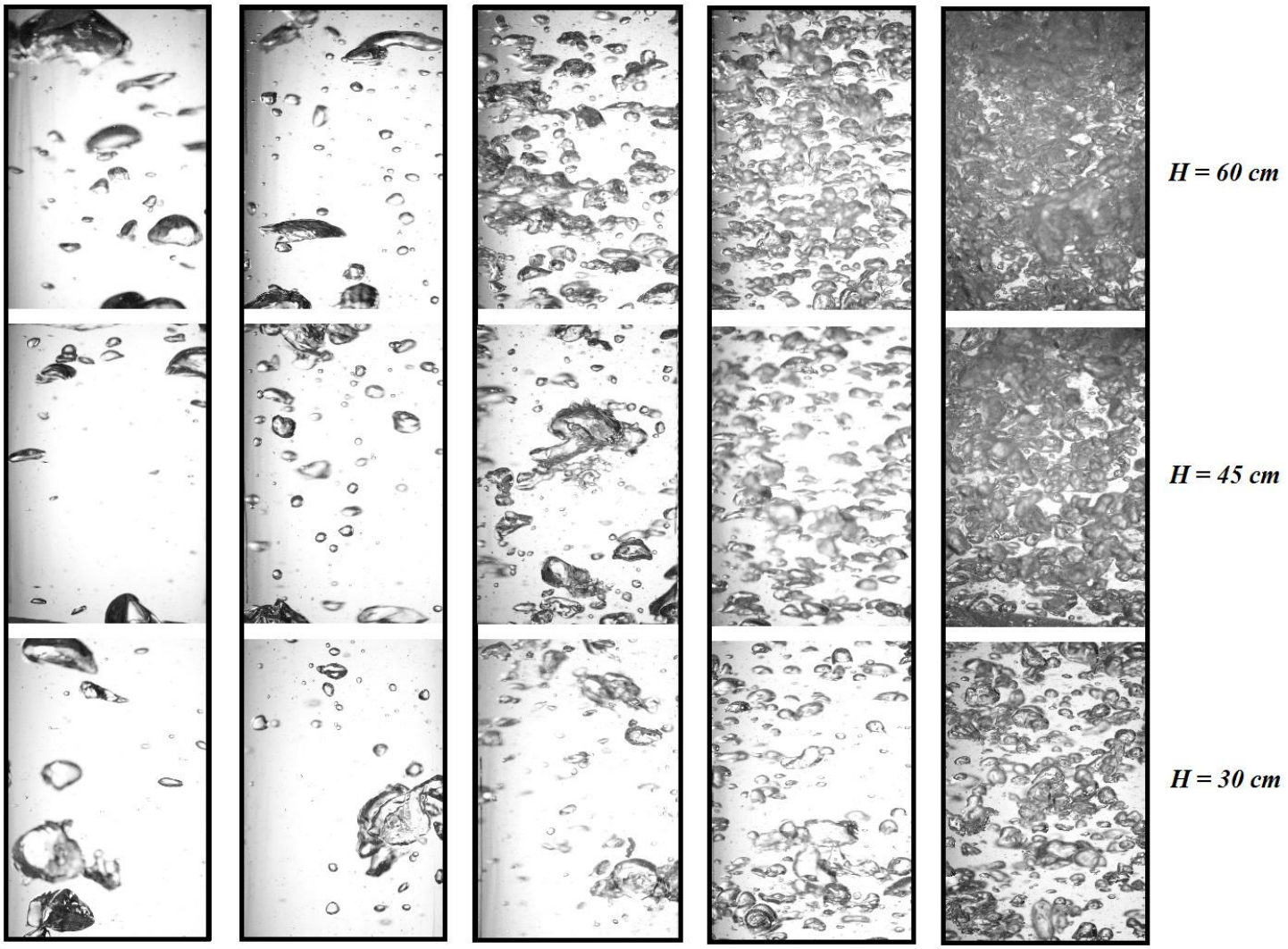

Figure 12: Bubble size distribution along column height at f = 10 Hz and (from left to right) A = 1.5 mm, 2.5 mm, 4.5 mm, 6.5 mm, 9.5 mm (H_0 = 85 cm, U_{SG} = 5.0 mm/s, p_e = 1 atm)

Some deviation from the log-normal, especially for smaller bubble sizes, agrees with a minimum bubble size suggested by the diminishing trend in Fig. 10 as the bubble size exhibits an approaching limit at $A/d_i > 6$. Therefore, there is an expected "cliff" in the distribution where very few bubbles are expected or observed to be smaller than the mean value ($D/d_i \approx 0.72$, Fig. 13). This size limit may be imposed by surface tension opposing the shearing force imposed by fluid oscillation [10, 23, 26].

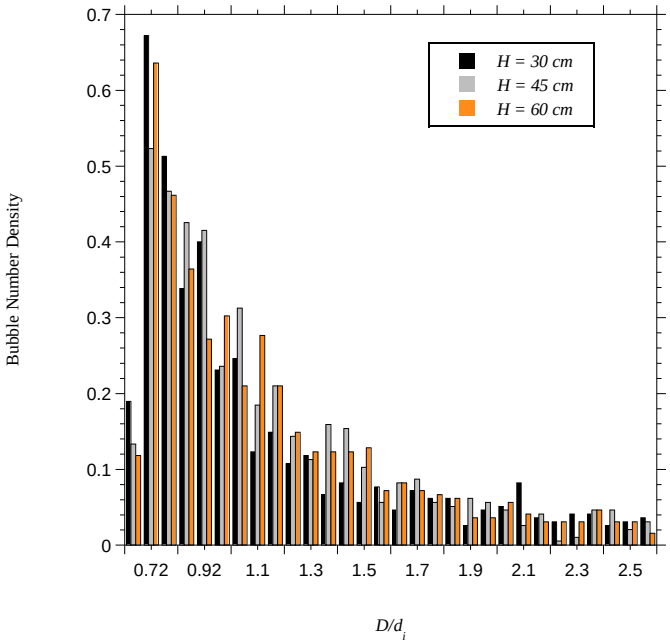

FIGURE 13. Dimensionless bubble diameter distribution as a function of column height for f = 12.5 Hz, A = 4.5 mm, U_{SG} = 5.0 mm/s, p_e = 1 atm

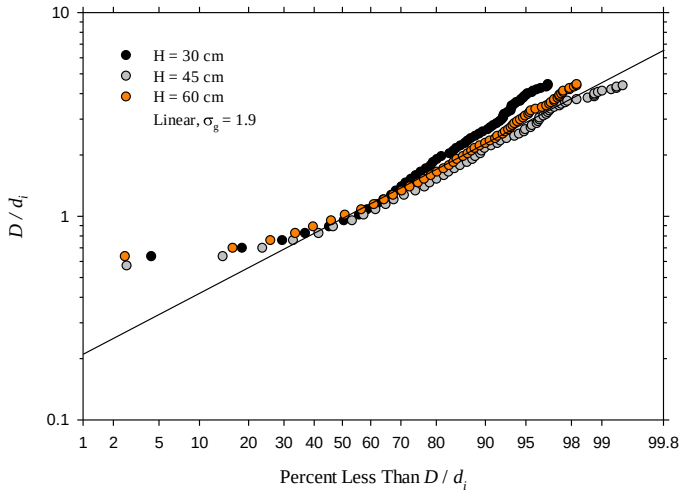

FIGURE 14. Dimensionless bubble diameter distribution as a function of column height for f = 12.5 Hz, A = 4.5 mm, U_{SG} = 5.0 mm/s, p_e = 1 atm

Observations of the bubble size distribution across the column diameter and along the height also showed an interesting result. Even though the bubbles were injected using a single point injector at the column center, at higher amplitudes the bubbles quickly "fanned out" to the column wall (Fig. 15). The fan out length (column height) was dependent on the frequency and amplitude setting and could be analogously viewed like an entrance effect in single phase pipe flow.

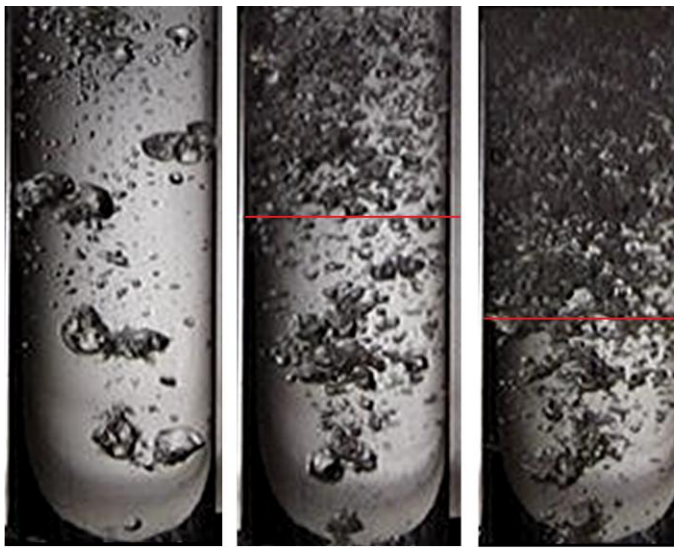

FIGURE 15. Entrance length effect of bubble distribution from single point injector at (from left to right) f = 10 Hz, f = 12.5 Hz and f = 15 Hz (A = 4.5 mm, U_{SG} = 5.0 mm/s, H_0 = 85 cm, p_e = 1 atm)

CONCLUSIONS

Mass transfer coefficient, void fraction, and bubble size data were collected for a vibration amplitude range of 1.5-9.5 mm at frequency ranges of 7.5-22.5 Hz. The vibration conditions at higher amplitudes had not been tested previously and experiments were performed to determine if separate influences exist on k_La, ε, and d_{32}. The results indicate special cases do exist for mass transfer improvement at reduced power requirements. Frequency maxima were observed similarly for both high and low amplitudes in the frequency range tested as noted in the literature. An optimum amplitude was observed to exist for k_La data, but not for void fraction.

The mass transfer and void fraction data were analyzed using regression and linear ANOVA methods to determine if a unifying parameter existed that could predict optimum BCR conditions. The results show that mass transfer can be predicted by a combination of superficial gas velocity, specific power input P_m, and Bjerknes number Bj. The correlation predicted for k_La is based on the same parameters proposed by a physics based model (Eq. 14), but the exponential values were significantly different, especially for P_m which showed a reduced influence than the theory. Data provided from previous research [16] was not statistically equivalent to the theory

proposed [14-15]. A new model is suggested based upon a linear ANOVA correlation of the data from both the present research and Waghmare [16] which predicts mass transfer coefficient as a function of U_{SG}, Bj and P_m. Void fraction data from the present research appeared to be highly influenced by the Bjerknes number, Bj contrary to the proposed theory of Eq.'s (13) and (25) while data from Waghmare [16] was confirmed to be influenced primarily by U_{SG} and P_m as predicted by the theory. The marked difference in void fraction results is not fully understood, but may be due to the method used to measure void fraction.

Bubble size distributions were determined from photographs taken at three column heights during vibration and static conditions. The results showed that d_{32} decreased with increasing frequency as expected, and increasing amplitude caused minimum bubble size to be reached at lower frequencies. The smallest bubble sizes (d_{32} ~ 3-4 mm) were obtained at high frequency/amplitude combinations, and size distributions were found to be log-normal. Similar log-normal distributions have been reported for bubble sizes directly measured by optical probes in static BCRs. Sauter mean diameter did not appear to exhibit local minimums due to frequency excitation modes with increasing vibration amplitude, except for f = 15Hz. However, bubble size was shown to continually decrease with increasing amplitude while mass transfer improvement decreased for larger amplitudes (A > 6.5 mm). Therefore, the data suggests it is not simply increasing interfacial surface area, a, which increases the product k_La, but rather the excitation modes established by specific frequency/amplitude combinations increase k_L by enhancing the diffusion mechanism.

ACKNOWLEDGMENTS

This work was funded by Sandia National Laboratories, Albuquerque, New Mexico through Dr. Timothy O'Hern. Sandia National Laboratories is a multi-program laboratory managed and operated by Sandia Corporation, a wholly owned subsidiary of Lockheed Martin Corporation, for the U.S. Department of Energy's National Nuclear Security Administration under contract DE-AC04-94AL85000. Special thanks go to Swanand Baghwat and Luke Walker for their assistance in this work.

NOMENCLATURE

A	Vibration amplitude (m)
A_{CS}	Cross section area (column) (m^2)
A_{proj}	Projected two dimensional area (m^2)
a	Interfacial surface area (m^{-1})
BCR	Bubble column reactor
Bj	Bjerknes number
C	Dissolved gas concentration (mg/L)
C_0	Initial dissolved gas concentration (mg/L)
C^*	Dissolved gas concentration at saturation or equilibrium (mg/L)
D	2D area equivalent bubble diameter (m)
$\mathscr{D}$	Diffusivity of the species (cm^2/s)
d_b	Bubble diameter (m)
d_{eq}	Area equivalent diameter (m)
d_{32}	Sauter mean diameter (m)
d_i	Gas injector internal diameter (m)
F	Force (time averaged) (N)
f	Vibration frequency (Hz)
g	Gravitational acceleration (m/s^2)
H	Dynamic air-liquid interface height (m)
H_L	Liquid column height (m)
H_0	Stagnant air-liquid interface height (m)
h	Liquid height above point of interest (m)
k_L	Liquid mass transfer coefficient (m/s)
k_La	Volumetric mass transfer coefficient (s^{-1})
k_La_0	Mass transfer coefficient at f = 0 Hz
$\dot{m}_G$	Gas mass flow rate (kg/s)
n	Bubble number (count)
P_m	Specific power input (W/kg)
P_v	Specific vibration power input (W/kg)
p_e	External or ambient pressure (Pa)
p_G	Gas pressure (Pa)
p_T	Total pressure (Pa)
p_0	Initial pressure (Pa)
R^2	Linear correlation coefficient
R_{air}	Specific ideal gas constant (J/kg-K)
T_G	Measured gas temperature (K)
t	Time (s)
U_{SG}	Superficial gas velocity (m/s)
V	Volume (m^3)
V_0	Initial bubble volume (m^3)
$\Delta V_{\max}$	Maximum bubble volume change (m^3)

Greek Symbols

ε	Column average void fraction
ε_0	Initial void fraction
ν	Kinematic liquid viscosity (m/s)
ρ_L	Liquid phase density (kg/m^3)
ρ_G	Gas phase density (kg/m^3)
σ	Liquid-gas surface tension (N/m)
σ_g	Geometric standard deviation of D/d_i samples
τ	Gas saturation time period (s)
ω	Vibration angular frequency (rad/s)

REFERENCES

[1] Harbaum, K.L., Houghton, G., 1960, "Effects of sonic vibrations on the rate of absorption of gases from bubble beds," Chemical Engineering Science, **18**, 90-92.

[2] Harbaum, K.L., Houghton, G., 1962, "Effects of sonic vibrations on the rate of absorption of carbon dioxide from bubble beds," Journal of Applied Chemistry, **12**, 234-240.

[3] Houghton, G., 1963, "The behavior of particles in a sinusoidal velocity field," Proceedings of the Royal Society of London, Series A, **272**(1348), 33-43.

[4] Bretsznajder, S., Jaszczak, M., Pasiuk, W., 1963, "Increasing the rate of certain industrial chemical processes by the use of vibration, International Chemical Engineering", **3** (4), 496-502.

[5] Buchanan, R.H., Jameson, G., Oedjoe, D., 1962, "Cyclic migration of bubbles in vertically vibrating liquid columns," I&EC Fundamentals, **1** (2), 82-86.

[6] Baird, M.H.I., 1963, "Resonant bubbles in a vertically vibrating liquid column," The Canadian Journal of Chemical Engineering, 52-55.

[7] Baird, M.H.I., Garstang, J.H., 1972, "Gas absorption in a pulsed bubble column," Chemical Engineering Science, **27**, 823-833.

[8] Krishna, R., Ellenberger, J., Urseanu, M.I., Keil, F.J., 2000, "Utilisation of bubble resonance phenomena to improve gas-liquid contact," Naturwissenschaften, **87**, 455-459.

[9] Krishna, R., Ellenberger, J., 2002, "Improving gas-liquid contacting in bubble columns by vibration excitement," International Journal of Multiphase Flow, **28**, 1223-1234.

[10] Ellenberger, J., Krishna, R., 2003, "Shaken, not stirred, bubble column reactors: Enhancement of mass transfer by vibration excitement," Chemical Engineering Science, **58**, 705-710.

[11] Ellenberger, J., van Baten, J.M., Krishna, R., 2005, "Exploiting the Bjerknes force in bubble column reactors," Chemical Engineering Science, **60**, 5962-5970.

[12] Knopf, F.C., Ma, J., Rice, R.G. and Nikitopoulos, D. (2005a), "Pulsing to improve bubble column performance: I. Low gas rates," AIChE Journal, **52** (3), 1103-1115.

[13] Knopf, F.C., Waghmare, Y., Ma, J., Rice, R.G., 2005, "Pulsing to improve bubble column performance: II. Jetting gas rates," AIChE Journal, **52** (3), 1116-1126.

[14] Waghmare, Y.G., Knopf, F.C., Rice, R.G., 2007, "The Bjerknes effect: Explaining pulsed-flow behavior in bubble columns," AIChE Journal, **53** (7), 1678-1686.

[15] Waghmare, Y.G., Rice, R.G., Knopf, F.C., 2008, "Mass transfer in a viscous bubble column with forced oscillations," Industrial and Chemical Engineering Research, **47**, 5386-5394.

[16] Waghmare, Y.G., 2008, "Vibrations for improving multiphase contact," Ph.D. Thesis, Dept. of Chemical Engineering, Louisiana State University, Baton Rouge, LA.

[17] Wu, C., Suddard, K., Al-Dahhan, M.H., 2008, "Bubble dynamics investigation in a slurry bubble column," AIChE Journal, **54** (4), 1203-1212.

[18] Xue, J., Al-Dahhan, M.H., Dudukovic, M.P., 2008, "Bubble velocity, size, and interfacial area measurements in a bubble column by four-point optical probe," AIChE Journal, **54** (2), 350-363.

[19] Xue, J., Al-Dahhan, M.H., Dudukovic, M.P., Mudde, R.F., 2008, "Four-point optical probe for measurement of bubble dynamics: Validation of the technique," Flow Measurement and Instrumentation, **19**, 293-300.

[20] Oliveira, M.S.N., Ni, X., 2001, "Gas hold-up and bubble diameters in a gassed oscillatory baffled column," Chemical Engineering Science, **56**, 6143-6148.

[21] Bjerknes, V.F.K., 1906, "Fields of force: Supplementary lectures, Applications to Meteorology," Reproduced by Cornell University Library, Ithaca, New York, Original by The Colombia University Press/The Macmillan Company, London.

[22] Jameson, G.J. and Davidson, J.F., 1966, "The motion of a bubble in a vertically oscillating liquid: theory for an inviscid liquid, and experimental results," Chemical Engineering Science, **21**, 29-34.

[23] Hinze, J.O., 1955, "Fundamentals of the hydrodynamic mechanism of splitting in dispersion processes," AIChE Journal, **1**, pp. 289-295.

[24] Rice, R.G., Barbe, D.T., Geary, N.W., 1990, "Correlation of nonverticality and entrance effects in bubble columns," AIChE Journal, **36** (9), 1421-1424.

[25] Clark, N.N., Atkinson, C.M., Flemmer, R.L.C., 1987, "Turbulent circulation in bubble columns," AIChE Journal, **33** (3), 515-518.

[26] Lewis, D.A. and Davidson, J.F., 1983, "Bubble sizes produced by shear and turbulence in a bubble column," Chem. Eng. Sci., **38** (1), 161-167.